2014 IEEE International Conference on Robotics & Automation (ICRA)
Hong Kong Convention and Exhibition Center
May 31 - June 7, 2014. Hong Kong, China

Development of a Hybrid Actuator with Controllable Mechanical Damping

Ioannis Sarakoglou, Nikos G. Tsagarakis, and Darwin G. Caldwell

Abstract— **This paper presents a novel hybrid actuator with controllable mechanical damping. It has been developed to provide subsequently the actuation means for haptic interfaces that can demonstrate intrinsic passive performance when rendering hard contacts. The overall actuator is a dual actuation system where one actuator is responsible for generating the joint motion while the second is dedicated to regulating the physical damping through a semi-active friction mechanism. This semi active friction mechanism applies a purely dissipative torque on the joint, which can be continuously controlled to render damping levels ranging from completely free to heavily damped and even a completely locked joint. The present work focuses mainly on the mechatronic details of the actuator design and in particular on the modelling and control of the damper. The proposed variable damping mechanism is evaluated in a simple 1-DOF joint. Experimental results are presented to demonstrate that the unit is capable of replicating physical damping with adequate performance.**

I. INTRODUCTION

Over time a number of key actuation technologies (electric, pneumatic, hydraulic, etc) have been used to power a variety of haptic feedback systems ranging from tactile feedback devices [1], desktop force feedback devices to full arm/hand exoskeleton systems [2],[3]. Of all actuator technologies the electric motor (DC or brushless DC motors) has been the most predominant approach. Transparency, force feedback fidelity and stability under a wide range of interaction parameters are all essential characteristics that any high performance haptic feedback device should posses. Actuators with high force bandwidth and low inertia; with low reduction ratio and low friction transmission systems, such as capstan drives, are usually integrated into light weight structures with optimized mechanical design to ensure transparency and force feedback fidelity. Although transparency and force fidelity can be partially achieved with the aforementioned design approaches, to concurrently ensure stability under a wide range of operating conditions and human interactions is a significant issue yet to be addressed.

The most common simulated surface constraint in haptics consists of a virtual spring and a virtual damper. It is well known that these virtual wall implementations when rendered through digital control of an electric motor can create instabilities. Virtual springs and dampers can appear also active when simulated, in contrast to their real counterparts who are always passive. These instabilities can be triggered by some erratic behaviour of the operator but have their root in intrinsic actuation, sensing and computational issues which affect their control. Such factors include the finite resolution of the sensors and their quantization noise [4], the existence of structural elasticity, the interaction between the discrete-time system (virtual wall force computation) and the continuous-time device/human operator [5]; the finite sampling rate and delays due to numerical integration [6] or other communication time delays between the haptic device and its controller or the slave tele-operated robot.

Apart from ensuring the fidelity of the interaction the stability of the haptic device is also critical for assuring the safety of the user in cases of powerful devices.

The stability region of virtual walls represented by virtual spring-damper systems was first studied by [7]. The analysis in [5],[8],[9] represents one of the studies in the literature towards a common stability condition for haptic displays. It has been shown experimentally that the stable region can be increased if the haptic device is physically damped [8],[9]. The approaches introduced in [10],[11],[12], consider time-domain passivity controllers where variable active damping is used to eliminate the energy generated by the haptic device. A more complex model of the haptic system including physical damping was investigated in [13]. It was demonstrated that higher physical damping allows for a larger stable virtual stiffness. Furthermore, for large values of the physical damping the maximum stable stiffness depends linearly on the sampling rate and the physical damping. The above studies and results suggest that an actuator with integrated variable physical damping may significantly improve the performance of a force feedback device when rendering hard contacts by intrinsically ensuring the device stability.

Looking at the relevant literature several semi-active damping systems have been proposed in various areas. Methods include friction based dampers[14] and magnetorheologial fluids [15],[16]. Semi-active adjustable dampers based on magnetorheologial fluids can provide variable damping levels on demand. However the introduction of liquids within the joint's structure complicates the mechanical design. In [17] the use of eddy currents provides nearly pure dissipative damping in terms of a force proportional to velocity. However the dissipative capacity of the system in very limited in terms of available damping torque. A more suitable implementation of semi-active damping, fitting the purpose of robotic applications, has been presented in [18] and [19]. This takes the form of a piezoelectric driven friction mechanism embedded in a compliant actuator.

I. Sarakoglou, N. G. Tsagarakis, Y. N. Karandikar and D. G. Caldwell are with the Department of Advanced Robotics, Istituto Italiano Di Tecnologia (IIT), Via Morego30, 16163 Genova, Italy, (phone:+3901071781274; fax:+39 010 720321); (e-mails: ioannis.sarakoglou@iit.it; nikos.tsagarakis@iit.it; darwin.caldwell@iit.it).

The current work presents the design and development of an actuator incorporating a semi-active variable damper. The implemented damper is a fast and strong friction mechanism with high dissipative capacity which can be controlled to modulate the apparent damping of the joint over a wide range. This paper is organized as follows. Section II presents the overall mechatronic design and the system architecture. Section III describes in detail the methods for designing the friction interface and produces a model of the system. Section IV presents the employed control scheme while section V presents the experimental results to validate the actuator functionality. Finally, section VI summarises the conclusions of this work.

II. System Description

A. Actuator Mechanical Assembly

The developed hybrid actuator consists of the main motor driving the joint and a damper mechanism controlled by a secondary actuator. A conceptual diagram of the system is presented in Figure 1. The joint motor drives the output link in a direct drive fashion, while the damper assembly provides damping in the form of controlled friction acting on the rare side of the main motor shaft. In this arrangement the damper is effectively connected in parallel to the output link with respect to ground (i.e. the actuator casing). A section view of the actuator is shown in Figure 2. The developed actuator is presented in Figure 3. It consists of two primary sub-assemblies, the main motor assembly and damper motor assembly. Starting from the left hand side the actuator in Figure 2 can be described as follows. The main motor assembly incorporates a frameless DC motor (Kollmorgen Model: QT-1406) with a custom casing and shaft. An optical incremental encoder with 40960 counts/rev (Model: MicroE 5340, CE300-4) is encased in the motor housing and provides position measurement of the rotor. The rotor shaft extends backwards providing a mounting location for the brake disk. The brake disk is attached to the joint motor shaft in a manner that it allows it to be clamped between the stationary pad and the movable pad upon actuation of the damper drive, shown graphically in Figure 1.

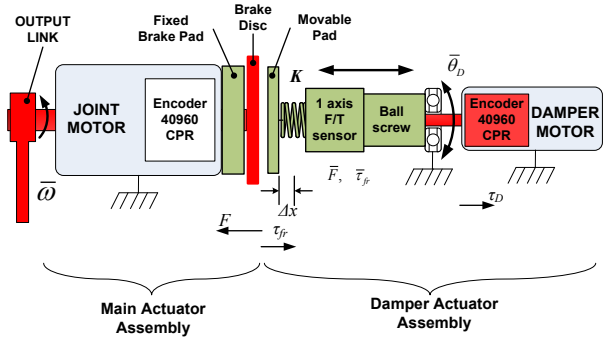

Figure 1 Conceptual schematic of the actuator and damper

The stationary brake pad is formed by an annular boss on the main motor casing, which has a clearance from the rotating disc. The disc is made thin and flexible in its central area and rigid on its perimeter in order to be able to flex backwards upon compression and to come into contact with the fixed pad. This limits the axial load put by the linear joint on the main motor shaft and allows for self-freeing of the disc. The movable pad is mounted on the linear joint and is driven by the damper motor assembly through a ball screw arrangement. As the ball screw extends the movable pad is pressed against the disk attached to the shaft of the main actuator which is then clamped on either side between the pads. The friction pads are made of aluminum while the disc is made of steel. The movable pad is mounted on the slider through a custom compliant element and a two-axis force/torque sensor. The compliant element is a spiral/volute spring designed to flex in and out of its plane, shown in Figure 3. It has a stiffness of ~320N/mm and is made of steel. It can deflect up to 1.5mm, beyond which it is mechanically locked for overload protection.

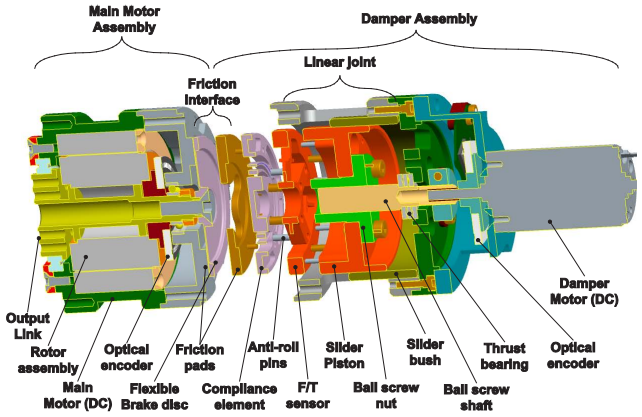

Figure 2 Exploded section view of the actuator

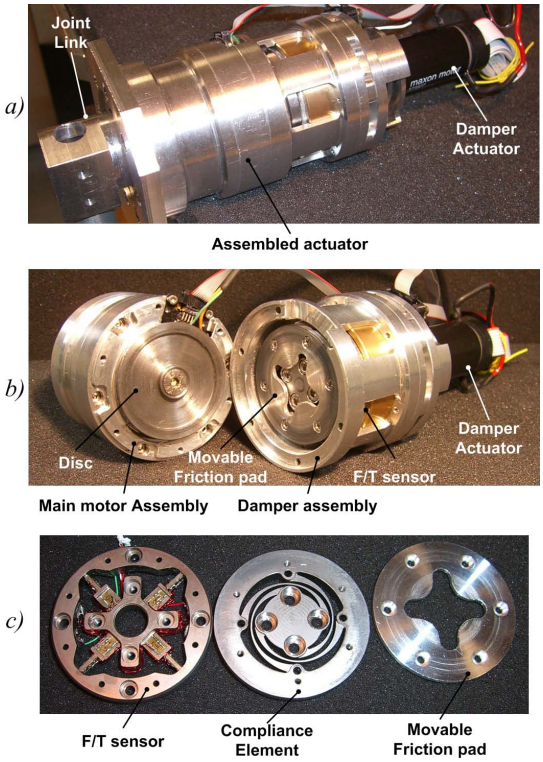

Figure 3 The developed variable damping actuator a) Complete assembly b) Main motor and damper assemblies exposing the brake disk, c) The F/T sensor, compliance element and movable friction pad.

With this stiffness and with the current position encoder the damper has a theoretical force resolution through position measurement of ~$7.8 \cdot 10^{-3}$N. Following the methods

presented subsequently in section III the theoretical resolution of the damping torque through position measurement is calculated at ~52·10^{-6}Nm. The compliant element is mounted at its centre to the force/torque sensor and at its perimeter to the movable friction pad. To block all rotations and unwanted deflection of the spring as a result of loads during damper operation, the compliant element is constrained to linear only deflection with 4 linear guide pins; the anti-roll pins visible in Figure 2. The linear joint assembly is further composed of the slider piston which is driven by the ball screw and slides in a brass bush constrained by two horizontal guide pins. A double direction thrust bearing takes the axial load off the damper motor and limits the shaft axial play. The damper motor is a gearless dc motor (Maxon 20W, RE25) with 297mNm stall torque, and an optical encoder identical to that of the main motor.

B. Force/Torque Sensor

The force-torque sensor shown in Figure 3 provides measurement of the normal force and of the friction torque applied by the movable pad on the disc. Its design is of the spokes on a hub type employing semiconductor strain gauges. Eight pairs of strain gauges are distributed on the 4 axisymmetric spokes forming two averaging signals which are sensitive to force and torque on the z axis. The force/torque sensor was calibrated using an ATI Mini45 force torque sensor in a modified assembly where both the sensors were mounted back to back inside the actuator. A plot of the sensor output after calibration against the Mini45, shown in Figure 4, indicates a good match and a successful calibration.

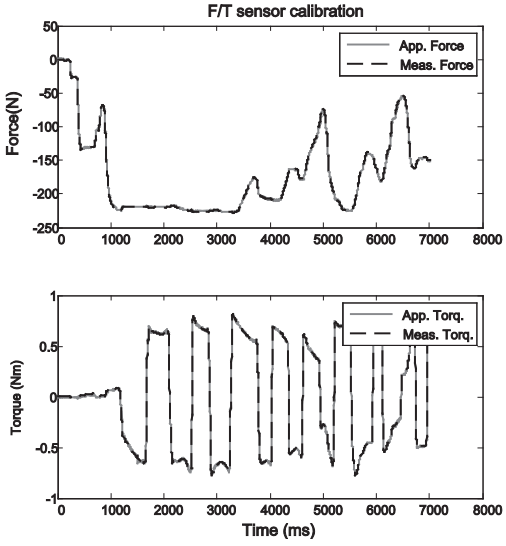

Figure 4 The sensor output versus an ATI Mini45 sensor.

C. System Architecture

The system architecture is presented in Figure 5. The two motors are controlled by two dedicated controller boards running 1kHz control loops and communicating over a LAN network. The host computer runs the high level control, commanding variables such as wall position, stiffness and damping of an interaction. These commands are transferred through UDP to the two controllers and are shared. In this implementation the main motor controller performs the position and stiffness control and passes its system states to the damper motor controller which controls friction for achieving the required damping.

III. Damper Design Method and Model

With reference to Figure 1, the torque of the damper motor τ_D is converted by the ball screw assembly into a normal force F which acts through the movable brake pad on the brake disc to produce the damping torque τ_{fr}. To compute design parameters such as friction surface geometry and actuator power, associated with the capacity of the friction mechanism to generate torque, we use the *uniform pressure theory*, which is relevant to clutches and brakes. With the aid of Figure 6 let us assume a friction surface as an annular sector A, formed by a rotating disc and a pad. From uniform pressure theory it can be shown (although omitted here for brevity) that for this type of friction surface geometry the effective friction torque τ_{fr} is described by:

$$\tau_{fr} = R\mu_k F \quad \text{where} \quad R = \frac{2(r_o^3 - r_i^3)}{3(r_o^2 - r_i^2)} \tag{1}$$

Where, for a moving system, μ_k is the coefficient of dynamic friction, F is the normal force and the product $\mu_k F$ is an equivalent friction generated on the friction surface A. R is the mean radius of the system obtained from r_i and r_o, which are the inner and outer radii of the pad. In this relationship, R in effect transforms the equivalent friction $\mu_k F$ into a torque at the mechanical axis O. In (2) the coefficient μ_{FT} is introduced, which describes the system's ability to transform normal force into torque [19] and we call it here the system's force-to-torque coefficient.

$$\tau_{fr} = \mu_{FT} F \quad \text{where} \quad \mu_{FT} = R\mu_k \tag{2}$$

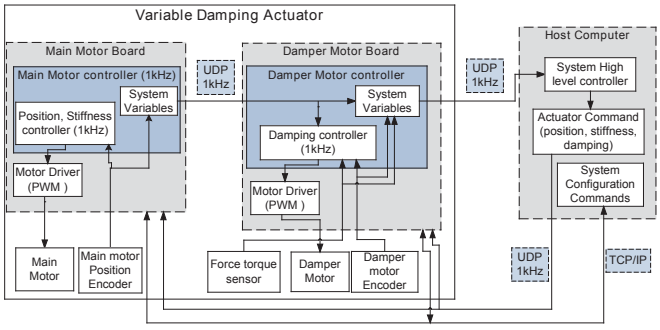

Figure 5 System architecture

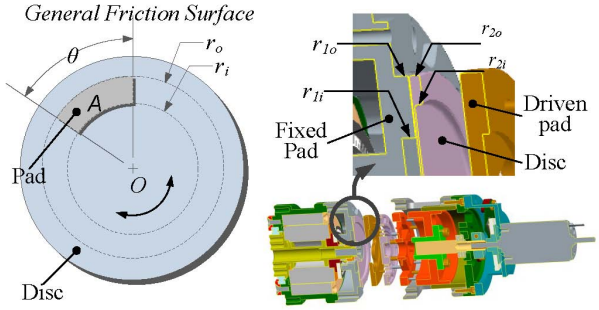

Figure 6 Friction surfaces formed by the brake disc and the pads.

TABLE I
COMPUTED FRICTION PROPERTIES OF THE TWO PADS

	Fixed Pad ($\kappa = 1$)		Movable Pad ($\kappa = 2$)	
$r_{\kappa i}$ **(m)**	$r_{1i} = 0.013$		$r_{2i} = 0.0175$	
$r_{\kappa o}$ **(m)**	$r_{1o} = 0.0215$		$r_{2o} = 0.0215$	
$\theta_{\kappa tot}$ **(rad)**	$\theta_{1tot} = 2\pi$		$\theta_{2tot} = 2\pi$	
R_κ**(m)**	$R_1 = 0.0176$		$R_2 = 0.0196$	
Surface condition	***Dry*** $_{(D)}$	***Lubricated*** $_{(L)}$	***Dry*** $_{(D)}$	***Lubricated*** $_{(D)}$
μ_k **(Alum.-Steel)**	$\mu_{kD} = 0.47$	$\mu_{kL} = 0.18$	$\mu_{kD} = 0.47$	$\mu_{kL} = 0.18$
$\mu_{FT\kappa} = \mu_k R_\kappa$ **(m)**	$\mu_{FT1(D)}$=0.0083	$\mu_{FT1(L)}$=0.0032	$\mu_{FT2(D)}$=0.0092	$\mu_{FT2(L)}$=0.0035
$\tau_{fr\_peak\_\kappa}$ **(Nm)**	*12.1822*	*4.6655*	*13.5453*	*5.1876*
$\tau_{fr\_cont\_\kappa}$ **(Nm)**	*1.2099*	*0.4634*	*1.3453*	*0.5152*

Table entries calculated with: ball screw pitch l=1mm, ball screw efficiency η=0.8, Damper motor stall torque τ_{D_stall}=0.297Nm, Damper motor continuous torque τ_{D_cont} =0.0291Nm.

TABLE II
COMPUTED FRICTION PROPERTIES OF THE DAMPER

	Dry $_{(D)}$	**Lubricated** $_{(L)}$
$\mu_{FT\_tot} = \mu_k R_{tot}$ **(m)**	$\mu_{FT\_tot(D)} = 0.0175$	$\mu_{FT\_tot(L)} = 0.0067$
$\tau_{fr\_tot\_peak}$**(Nm)**	25.73	9.85
$\tau_{fr\_tot\_cont}$**(Nm)**	2.56	0.98

Although the angle θ and the area A of the annular sector are used in the derivation of (1), they do not appear in this equation, which describes the transformation of force into torque by friction. This is in accordance with Amonton's second law according to which, macroscopically, friction is independent of the area of contact. However, A would indeed become relevant when considering operation over long periods of time and for high levels of dissipative work where heat is produced at a high rate. The transfer of heat generated at the frictional interface into the system's surroundings should be expected to mainly take place by conduction and would be proportional to the contact area A. Therefore A should be large enough to assist heat transfer preventing temperature build up at the contact, which would lead to excessive wear and alteration of material properties including the coefficients of friction.

For multiple friction surfaces κ with the same friction coefficient and one commonly applied normal force F, the total available friction torque τ_{fr_tot} is proportional to the normal force and the total mean radius R_{tot} of the system, (3). R_{tot} is the sum of the individual mean radii R_κ of the friction surfaces (4). The conversion of the damper motor torque τ_D into normal force F through the ball screw is given by (5), where l and η are the pitch and the efficiency of the ball screw. Finally the relationship between the damper motor torque and the generated friction torque is given by (6). It is obvious that (6) has a meaning only when the output link is moving or when the damper is balancing a torque applied on it through static friction, in which case the static friction coefficient should be used.

With the above methodology the damper actuator was designed and the transmission and actuation components were selected. The adopted geometry for the friction interface and the calculated frictional properties of the two pads for the cases of a dry and a lubricated contact, are listed in TABLE I. The system's force to toque coefficient μ_{FT_tot} and the total friction torque capacity τ_{fr_tot} are summarized in TABLE II. In the implemented system the friction surfaces were lubricated for a smoother operation. According to these characteristics the available friction torque is enough to control damping and to even completely brake the main actuator.

$$\tau_{fr\_tot} = R_{tot}\mu_k F \quad \text{or} \quad \tau_{fr\_tot} = \mu_{FT\_tot} F \tag{3}$$

$$R_{tot} = \sum_{\kappa=1}^{n} R_\kappa = \sum_{\kappa=1}^{n} \frac{2(r_{\kappa o}^3 - r_{\kappa i}^3)}{3(r_{\kappa o}^2 - r_{\kappa i}^2)} \quad \text{and} \quad \mu_{FT\_tot} = R_{tot}\mu_k \tag{4}$$

$$F = \frac{\tau_D 2\pi\eta}{l} \tag{5}$$

$$\tau_{fr\_tot} = \frac{\mu_{FT\_tot}\tau_D 2\pi\eta}{l} \tag{6}$$

IV. Damper System Control

The aim of the damper control system is to control damping by modulating the torque τ_{fr_tot} applied to the output link according to (7). Where, $\dot{\theta}_M$ is the velocity of the output link and C_{app} is the damping coefficient realized with the regulation of τ_{fr_tot}, C_{sys} is the inherent damping coefficient of the link and C_{req} is the total damping coefficient required for the link. From (3) and (7) the relationship between the applied normal force F and the link's damping is given in (8). Although damping could be regulated by directly controlling the applied force or torque using the force/torque sensor signal, as shown in (7) and (8), in this work it is performed by regulating the position of the damper motor. The reason is that both friction and normal force would be both problematic signals at the boundary of a rigid-free contact. This contact boundary exists in the system by design, since while the damper is retracting backwards it can attain positions where the movable pad looses contact with the disc and is traveling in free space. During free space travel, the force and torque seen at the sensor should be zero. Therefore at the event of loss of contact between the movable pad and the disc force and torque would become uncontrollable. To avoid hard contacts and the aforementioned nonlinearity the system incorporates a compliant element (discussed previously and shown in Figure 2 and Figure 3). In the current implementation it has a stiffness of 320 N/mm and a deflection of 1.5mm, which provides enough resolution and range (see section II.A) for position control of the system. Therefore position becomes the means to modulate the applied force, circumventing the problem of force and torque nonlinearity at the point of contact θ_C.

Considering the conversion of rotation into translation via the ball screw, the normal force is related to angular position as shown in (9). Where K_{rot} is an equivalent coefficient of stiffness along the ball screw displacement with units *N/rad*, θ_{def} is the equivalent angular deflection of the spring, θ_D is the angular position of the damper motor, and θ_C is the angular position of the damper motor when the movable pad initially contacts the disc. The equivalent rotational stiffness K_{rot} is obtained by taking position measurements at the damper's encoder and force measurements form the sensor adjacent to the movable pad, shown in Figure 7. This equivalent stiffness K_{rot} includes the stiffness of the compliant element, the

stiffness of the force torque sensor and the stiffness of the housing structure. A 6th order polynomial fit is used to model the stiffness at forces lower than 10N where it appears nonlinear. Finally the required damping C_{req} is controlled by regulating the angular position of the damper motor θ_D to achieve the required angular deflection θ_{def} according to the equivalent stiffness K_{rot} and the position θ_C of pad to disc contact, shown in (10).

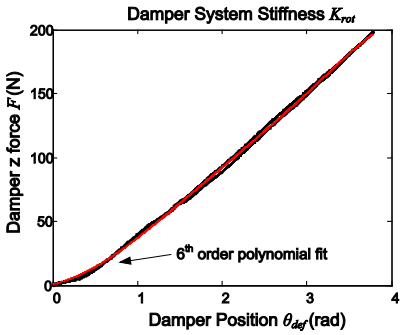

Figure 7 Eqivalent rotational stiffness K_{rot} (*N/rad*) of the system.

$$\tau_{fr\_tot} = C_{app}\left|\dot{\theta}_M\right| \text{ with } C_{app} = C_{req} - C_{sys} \tag{7}$$

$$F = \frac{(C_{req} - C_{sys})\left|\dot{\theta}_M\right|}{\mu_{FT}} \tag{8}$$

$$F = K_{\text{rot}}\theta_{def} \text{ with } \theta_{def} = \theta_D - \theta_C \tag{9}$$

$$\theta_D = \theta_C + \frac{(C_{req} - C_{sys})\left|\dot{\theta}_M\right|}{\mu_{FT} K_{\text{rot}}} \tag{10}$$

$$C_{app} = \frac{\tau_{fr1\_meas} + \mu_{FT2} F_{meas}}{\left|\dot{\theta}_M\right|}, \ \dot{\theta}_M \neq 0 \tag{11}$$

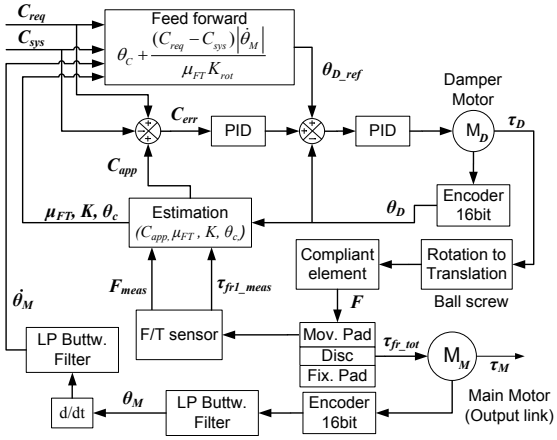

Figure 8 Control diagram of the damper system

The overall system control diagram is shown in Figure 8. Tracking of θ_D is performed with a PID controller which regulates position according to θ_{D_ref} generated by the feed forward block. The applied damping C_{app} can be estimated online according to (11), where τ_{fr1_meas} and F_{meas} are the friction torque and normal force measured at the movable pad by the force torque sensor. Tracking of the damping coefficient C_{req} is finally implemented in an outer PID loop which minimises the error based on an estimation of the applied damping C_{app}.

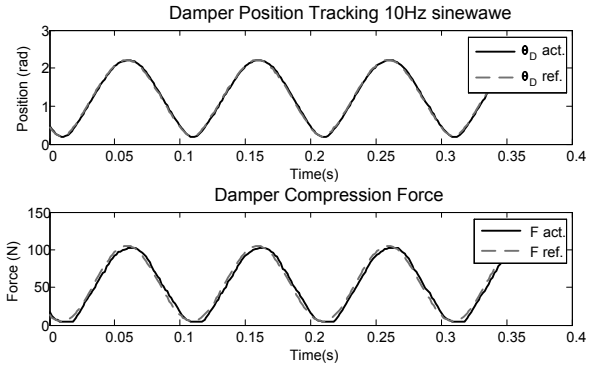

Figure 9 Tracking performance of the damper motor.

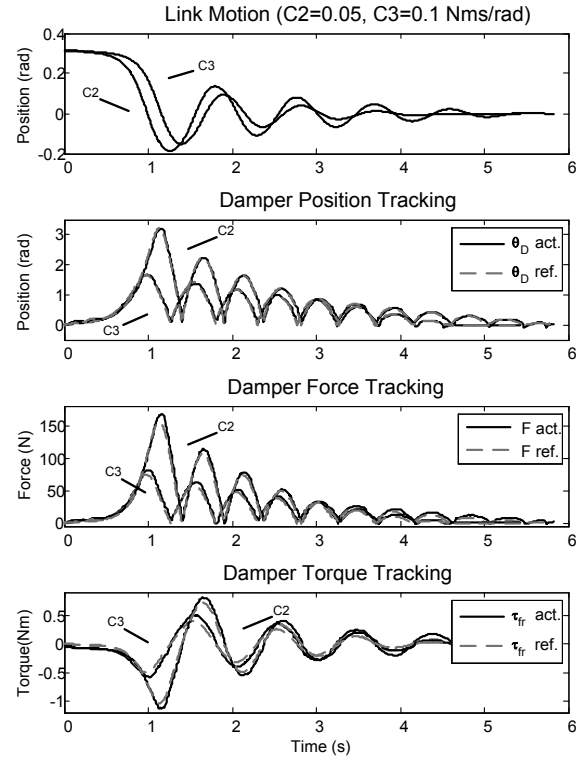

Figure 10 Damper plots for a pendulum mass=1kg at 0.2m subjected to damping C_2=0.05Nms/rad and C_3=0.1Nms/rad.

V. Experimental Results

The response of damper motor to a sinusoidal reference is shown in Figure 9. It can be noticed that position tracking is very good, while also the measured force is also close to that computed with the stiffness model. To evaluate the performance of the damper a pendulum experiment was performed. The output shaft was connected through a rigid link to a mass of 1kg, which was allowed to oscillate from a high vertical position (180°) to rest at 0°. Since the main actuator was not the focus of this work it was kept inactive during the course of these experiments. Data for two damping coefficients, namely C_2 and C_3 are presented in Figure 10.

Finally the ability of the system to achieve the commanded damping coefficients C_1=0.01, C_2=0.05 and C_3=0.1 Nm-s/rad is demonstrated in Figure 12.

To validate the design assumptions with respect to the friction properties of the system the μ_{FT} coefficient was obtained experimentally during the pendulum experiment. A plot of the measured torque against the measured force, is shown in Figure 11. This experimentally measured value for μ_{FT_tot} varies for the positive and negative directions by 6%. Furthermore, the measured μ_{FT_tot} is larger compared to the calculated value in TABLE II by 15% and 7% for the positive and negative directions respectively. This apparent direction dependence in the measured force-to-torque coefficient μ_{FT_tot} could be the result of mechanical inaccuracies in the actuator assembly or may emanate from sensor nonlinearity in this region of load.

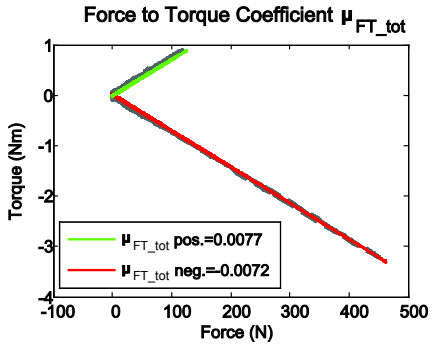

Figure 11 Experimental evaluation of the friction to torque coefficient μ_{FT}

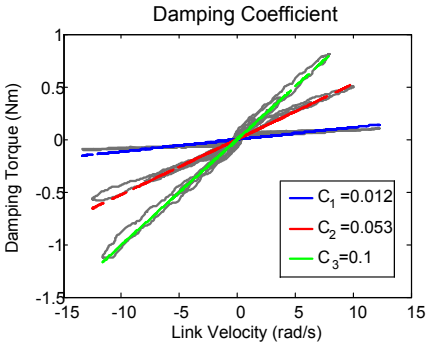

Figure 12 Damping coefficients obtained from the pendulum experiment.

VI. Conclusion and Future Work

This paper presented the design and development of an actuator with variable damping in the form of a controllable semi-active friction mechanism. The mechatronic components of the actuator have been described in detail including the mechanical design of the actuator, the damper assembly and the various sensing and computation units. The theoretical method for designing the damper's friction unit and has been presented and a model of the system's friction and stiffness has been developed. A control scheme, where friction is controlled through position using the stiffness-friction model has been described. The proposed variable damper mechanism has been evaluated on a simple 1-DOF joint. The experimental results verified the design method since the measured characteristics of the damper match to a large extent the design calculations. Furthermore the results have demonstrated that the unit is fast and powerful enough to achieve the required damping. Further work will concentrate on integrating this actuator into a haptic device and controlling both the damper and the main actuator for the purpose of simulating stable stiff haptic contacts.

Acknowledgment

The research leading to these results has received funding from the European Union Seventh Framework Programme FP7/2007-2013 under grant agreement n° 601165 of the projects ``WEARHAP - WEARable HAPtics for humans and robots" and SAPHARI FP7-ICT-287513.

References

[1] I. Sarakoglou, *et al.*, "A compact tactile display suitable for integration in VR and teleoperation," in *Proc. IEEE Int. Conf. Robotics and Automation (ICRA)*, St. Paul, MN, 2012, pp. 1018-1024.

[2] D. G. Caldwell, *et al.*, ""Soft" Exoskeletons for Upper and Lower Body Rehabilitation - Design, Control and Testing," *International Journal of Humanoid Robotics,* vol. 4, pp. 549-573, 2007.

[3] I. Sarakoglou, *et al.*, "Exoskeleton-Based Exercisers for the Disabilities of the Upper Arm and Hand " in *Rehabilitation Robotics*, S. S. Kommu, Ed., ed Vienna, Austria: I-Tech Education and Publishing, 2007, pp. 499-522.

[4] J. E. Colgate, *et al.*, "Issues in the haptic display of tool use," in *Proc. IEEE/RSJ International Conference on Intelligent Robots and Systems 95. 'Human Robot Interaction and Cooperative Robots'*, Pittsburgh, 1995, pp. 140-145 vol.3.

[5] J. E. Colgate and G. Schenkel, "Passivity of a class of sampled-data systems: Application to haptic interfaces," in *Proc. American Control Conf., Baltimore, MD*, ed, 1994, pp. 3236 -3240.

[6] E. Guglielmino, *et al.*, " Damp-by-wire: Magnetorheological vs Friction Dampers," in *16th IFAC World Congress*, ed. Prague, 2005.

[7] S. Salcudean and T. Vlaar, "On the emulation of stiff walls and static friction with a magnetically levitated input/output device," in *ASME Journal of Dynamic Systems, Measurement and ControlD*, ed, 1997.

[8] J. Mehling, *et al.*, "Increasing the impedance range of a haptic display by adding electrical damping," in *in Proc. of the IEEE WorldHaptics Conference (WHC).* ed, 2005, pp. 257 -262.

[9] J. E. Colgate and J. Brown, "Factors affecting the z-width of a haptic display," in *ICRA*, ed, 1994, pp. 3205-3210.

[10] B. Hannaford and J. Ryu, "Time-domain passivity control of haptic interfaces," in *ICRA*, ed, 2001, pp. 1863 -1869.

[11] J. Ryu, *et al.*, "Time-domain passivity control of haptic interfaces," in *ICRA*, ed, 2003, pp. 822 -827.

[12] J. Ryu, *et al.*, "Time domain passivity control with reference energy behavior," in *IEEE Transactions on Control Systems Technology*, ed, 2005.

[13] T. Hulin, *et al.*, "Stability boundary for haptic rendering: Influence of physical damping," in *Proc. IEEE/RSJ Int. Conf. on Intelligent Robots and Systems, (IROS)*, ed, 2006, pp. 1570 -1575.

[14] E. Guglielmino and K. A. Edge, "Modelling of an electrohydraulically-activated friction damper in a vehicle application," presented at the ASME International Mechanical Engineering Congress & Exposition New York, USA, 2001.

[15] E. Guglielmino, *et al.*, "Damp-by-wire: magnetorheological vs. friction dampers," presented at the International Federation of Automatic Control (IFAC) 16th World Congress, Prague, Czech Republic, 2005.

[16] M. Unsal, *et al.*, "Two semi-active approaches for vibration isolation: piezoelectric friction damper and magnetorheological damper," presented at the IEEE International conference on Mechatronics, 2004.

[17] A. H. Gosline, *et al.*, "On The Use of Eddy Current Brakes as Tunable , Fast Turn-On Viscous Dampers For Haptic Rendering," in *Proc. Eurohaptics*, 2006, pp. 229-234.

[18] M. Laffranchi, *et al.*, "A Variable Physical Damping Actuator (VPDA) for Compliant Robotic Joints," in *Proc. International Conference on Robotics and Automation (ICRA)*, 2010.

[19] M. Laffranchi, *et al.*, "Analysis and Development of a Semiactive Damper for Compliant Actuation Systems," *Mechatronics, IEEE/ASME Transactions on,* vol. 18, pp. 744-753, 2013.